MULTI-EXPOSURE IMAGE FUSION METHOD USING RESULTANT IMAGES OF HISTOGRAM SPECIFICATION

Yoshiaki Ueda[1,*], Daiki Moriyama[2] and Noriaki Suetake[3]

[1]Department of Applied Mathematics
Faculty of Science
Fukuoka University
8-19-1, Nanakuma, Jonan-ku, Fukuoka 814-0180, Japan
*Corresponding author: uedayos@fukuoka-u.ac.jp

[2]Izumo Murata Manufacturing Co., Ltd.
2308, Kaminaoe, Hikawa-cho, Izumo City, Shimane 699-0696, Japan

[3]Graduate School of Science and Technology for Innovation
Yamaguchi University
1677-1, Yoshida, Yamaguchi 753-8512, Japan

ABSTRACT. *In this letter, we propose a histogram specification-based multi-exposure image fusion method. In the proposed method, for the under- and over-exposure pixel whose hue component tends to be improper, the replacement of a hue component by the pixel, which has an appropriate intensity, is achieved first. Then, the histogram specification using a triangular-shaped target histogram is executed. Its output and an original image are blended while preserving the saturation component to obtain well-enhanced multi-exposure images. Finally, the resultant image with good visual quality is obtained by saturation-based weighted averaging of enhanced multi-exposure images. Experimental results show that the proposed method has better performance in comparison with conventional methods.*
Keywords: Multi-exposure image fusion, Histogram specification, Hue correction, Saturation preservation

1. **Introduction.** The dynamic range of human light perception for natural scenes is wider than those of digital cameras. When a digital camera takes an image of a natural scene, the image may contain under-exposed or over-exposed regions. For this reason, to obtain contrast improved images, digital cameras have functions to create a high dynamic range (HDR) image by using multi-exposed images [1, 2, 3, 4, 5, 6].

In many cases, multi-exposure images contain under- and over-exposed regions. These regions consist of extremely dark or bright pixels whose hue components are not reliable. When HDR images are generated, multi-exposure images are fused using pixel-wise weight, and then the under- and over-exposed regions are also used. Therefore, if such regions, in multi-exposure images, are converted and better gradation expression is obtained, it is considered that the visual quality of the generated HDR image will be good.

Histogram equalization (HE) [7] is one of the contrast enhancement methods for digital images. HE can automatically calculate the tone mapping function so that the resultant image has uniform intensity distribution. As a generalization of histogram equalization, there is the histogram specification method. Histogram specification can automatically calculate the tone mapping function so that the resultant image has a specified histogram shape. The histogram specification method is based on input and target intensity

distributions and their cumulative distributions. The extended versions of histogram specification-based methods are proposed [8, 9, 10, 11, 12].

This letter proposes a novel multi-exposure image fusion method consisting of hue correction, histogram specification-based intensity conversion while preserving saturation, and saturation-based weighted averaging. The novelty of this research is that the hue of each pixel of the multi-exposure image is replaced with the hue of the highly reliable pixel of the multi-exposure image before fusion. By introducing hue correction and saturation preserving, it is expected to prevent the occurrence of unnatural colors when intensity conversion is performed. Furthermore, the proposed method's advantage is that the HDR image can be generated by using a weighted sum of more reliable pixel values, which are obtained by using the histogram specification method. The histogram specification method has the advantage that visual deterioration is unlikely to occur because the tone mapping curve can be controlled. Experiments using various images are performed to verify the effectiveness of the proposed method.

The rest of this paper is structured as follows. In Section 2, we present our multi-exposure image fusion method, including hue correction, intensity conversion, saturation preserving, and fusion of multi-exposure images. Section 3 describes experimental results and evaluations for some multi-exposure images. Finally, the conclusion and future research directions remarks are given in Section 4.

2. **Proposed Method.** Figure 1 shows examples of multi-exposure images. As shown in Figures 1(a) and 1(d), both the intensity contrast and saturation of the under-exposure image are very low. Its intensity distribution is extremely biased to the dark region. On the other hand, the over-exposure image is saturated, and its intensity distribution is biased to the bright region, as shown in Figures 1(c) and 1(f), respectively. To obtain a fusion image having a good visual quality, it is required hue correction and intensity enhancement of multi-exposure images before executing the image fusion procedure.

In the proposed method, well-enhanced multi-exposure images are obtained firstly. Then, they are combined by using the saturation-based weights to get the fusion image. Concrete procedures of the proposed method are explained as follows.

2.1. **Hue correction.** In multi-exposure images, over-exposed and under-exposed pixels are contained. In such pixels whose intensities are close to 0 or 255, the hue information is often lost. On the other hand, the pixels whose intensities are close to 128 contain relatively correct hue information. Therefore, the hue components of all (i, j)-th pixels are replaced by that of the (i, j)-th pixel whose intensity is the closest to 128 among multi-exposure images.

At first, an intensity $x_{\text{int}}^{(l)}(i, j)$ of the (i, j)-th pixel of the l-th exposure image ($l = 1, 2, \ldots, L$) is calculated as $\left(r_{\text{ori}}^{(l)}(i, j) + g_{\text{ori}}^{(l)}(i, j) + b_{\text{ori}}^{(l)}(i, j) \right) \big/ 3$, where $r_{\text{ori}}^{(l)}(i, j)$, $g_{\text{ori}}^{(l)}(i, j)$, and $b_{\text{ori}}^{(l)}(i, j)$ stand for R, G, and B components of the (i, j)-th pixel of the l-th original exposure image, respectively. Then, the hue correction is achieved as follows:

$$x_{\text{hue}}^{(l)}(i, j) = x_{\text{hue}}^{(l^*)}(i, j), \tag{1}$$

$$l^* = \operatorname*{arg\,min}_{l \in \{1, \ldots, L\}} \left| x_{\text{int}}^{(l)}(i, j) - 128 \right|. \tag{2}$$

This procedure is executed in HSV color space, and the hue corrected images replace the original multi-exposure ones. Here, the (i, j)-th pixel of l-th hue corrected image is denoted as $\boldsymbol{x}^{(l)}(i, j) = \left(r^{(l)}(i, j), g^{(l)}(i, j), b^{(l)}(i, j) \right)$.

Figure 2 shows a comparison between the intensity enhanced image with and without hue correction. If intensity enhancement is applied to a multi-exposure image before hue correction, we can see that the walls are greenish, as shown in Figure 2(b). On the other
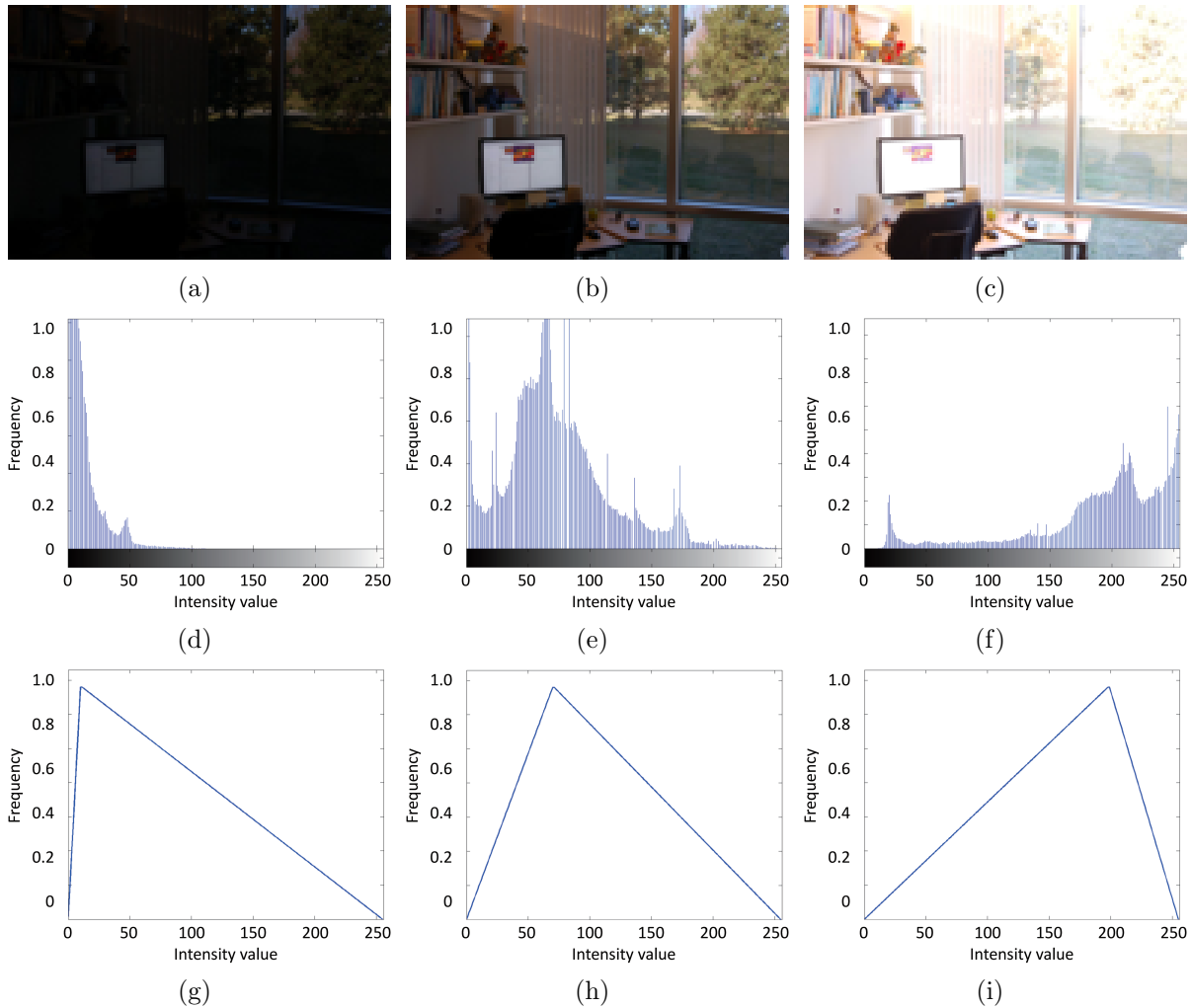
FIGURE 1. Examples of multi-exposure images and their histograms: (a) under-exposure image, (b) middle-exposure image, (c) over-exposure image, (d) histogram of (a), (e) histogram of (b), (f) histogram of (c), (g) triangular-shaped histogram for (a), (h) triangular-shaped histogram for (b), and (i) triangular-shaped histogram for (c)

hand, if intensity enhancement is applied to multi-exposure image after hue correction, the wall has a natural color, as shown in Figure 2(d).

2.2. **Intensity conversion.** In the intensity conversion procedure, contrasts of the multi-exposure images are improved by the histogram specification. The pixel intensities distribute widely toward the center of the intensity range. Concretely, in the histogram specification, as a target histogram $h_{\text{tar}}^{(l)}(u)$, $u \in \{0, \ldots, 255\}$ for the l-th exposure image, a mixture of an original intensity histogram $h^{(l)}(u)$ and a triangular-shaped histogram $h_{\text{tri}}^{(l)}(u)$ is used as follows:

$$h_{\text{tar}}^{(l)}(u) = \alpha h_{\text{tri}}^{(l)}(u) + (1 - \alpha)h^{(l)}(u), \tag{3}$$

$$\alpha = 1 - \min\left\{\frac{V^{(l)}}{V_{\text{tri}}^{(l)}}, 1\right\}. \tag{4}$$

Figures 1(g), 1(h), and 1(i) show examples of the triangular-shaped unimodal histograms corresponding to multi-exposure images shown in Figures 1(a), 1(b), and 1(c), respectively. The shape of triangular histogram corresponding to the l-th exposure image is
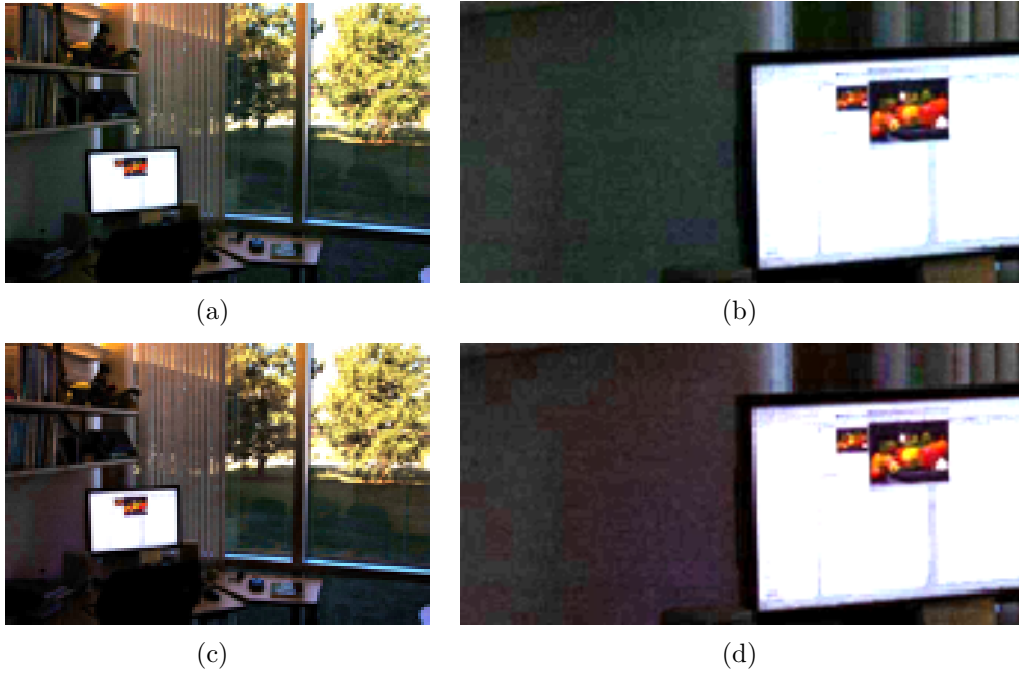
FIGURE 2. (color online) Comparison after intensity enhancement with and without hue correction: (a) enhanced image without hue correction, (b) enlarged image of (a), (c) enhanced image with hue correction, and (d) enlarged image of (c)

decided by 0, 255, and the mean intensity $\mu_{\text{int}}^{(l)}$. In Equation (4), $V_{\text{tri}}^{(l)}$ is the intensity variance of the triangular histogram, and $V^{(l)}$ is the intensity variance of the original image. In the proposed method, α is automatically determined based on the intensity variance. When $V^{(l)} \simeq V_{\text{tri}}^{(l)}$ is satisfied, α is set to approximately 0, and the conversion becomes close to an identity transformation. On the other hand, when $V^{(l)} \ll V_{\text{tri}}^{(l)}$ is satisfied, α is set to approximately 1. The shape of the target histogram becomes similar to the triangular-shaped histogram, and the contrast of the image is strongly enhanced. After setting of target histogram, the histogram specification is applied to $x_{\text{int}}^{(l)}(i,j)$, and intensity converted images $x_{\text{int}}'^{(l)}(i,j)$ are obtained. Then, the local contrast correction is performed to the pixels with intermediate intensity levels. The local contrast corrected result $x_{\text{int}}''^{(l)}(i,j)$ is obtained as follows:

$$x_{\text{int}}''^{(l)}(i,j) = \beta^{(l)}(i,j)x_{\text{int}}'^{(l)}(i,j) + \left(1 - \beta^{(l)}(i,j)\right)x_{\text{int}}^{(l)}(i,j), \tag{5}$$

$$\beta^{(l)}(i,j) = \min\left\{\left|\frac{m^{(l)}(i,j) - \mu_{\text{int}}^{(l)}}{\mu_{\text{int}}^{(l)}}\right|, 1\right\}, \tag{6}$$

where $m^{(l)}(i,j)$ is a result of a Gaussian-filtering with $[2r+1, 2r+1]$ window for the image $x_{\text{int}}^{(l)}(i,j)$. To convert the intensity of $\boldsymbol{x}^{(l)}(i,j)$, the ratio of $x_{\text{int}}''^{(l)}(i,j)$ and $x_{\text{int}}^{(l)}(i,j)$ is multiplied to $\boldsymbol{x}^{(l)}(i,j)$ as follows:

$$\boldsymbol{x'}^{(l)}(i,j) = \frac{x_{\text{int}}''^{(l)}(i,j)}{x_{\text{int}}^{(l)}(i,j)}\boldsymbol{x}^{(l)}(i,j). \tag{7}$$

Equation (7) satisfies Naik and Murthy's hue preserving condition [13].

2.3. **Saturation preserving.** In Equation (7), the hue is preserved, but the saturation is not preserved. Then the image impression might be changed drastically. Therefore, the saturation preserving procedure is conducted so that the saturation before and after
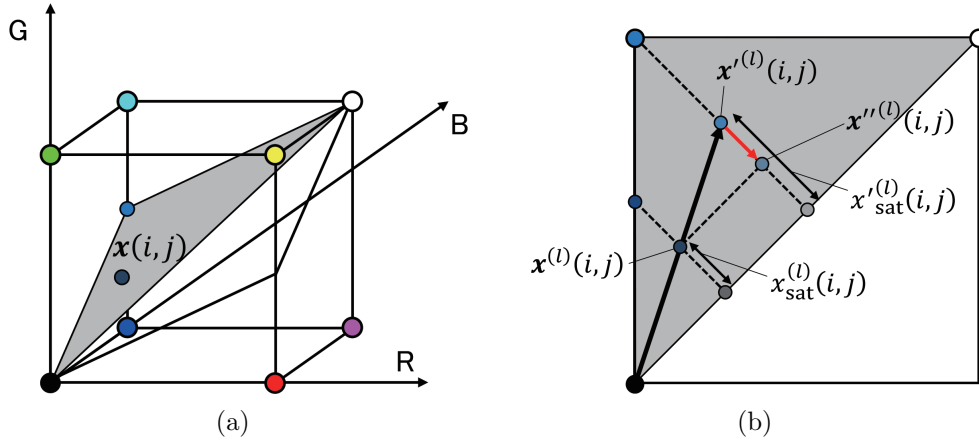
FIGURE 3. Schematic diagram of RGB color space and constant hue plane: (a) RGB color space, and (b) constant hue plane

intensity conversion does not change. Figure 3 shows a schematic diagram of the RGB color space and the constant hue plane. Figure 3(a) shows that the triangle consists of black $(0, 0, 0)$, white $(255, 255, 255)$, and maximally saturated color whose hue is the same as $\boldsymbol{x}$. The triangle is called a constant hue plane. Figure 3(b) is a schematic diagram of the constant hue plane. In Figure 3(b), $x_{\text{sat}}^{(l)}(i, j)$ and $x_{\text{sat}}'^{(l)}(i, j)$ represent the saturations of $\boldsymbol{x}^{(l)}(i, j)$ and $\boldsymbol{x}'^{(l)}(i, j)$, respectively. The saturation is calculated as follows:

$$x_{\text{sat}}^{(l)} = \sqrt{\frac{\left(r^{(l)} - g^{(l)}\right)^2 + \left(g^{(l)} - b^{(l)}\right)^2 + \left(b^{(l)} - r^{(l)}\right)^2}{3}}, \tag{8}$$

where (i, j) is omitted to save the space. The saturation-preserved pixel $\boldsymbol{x}''^{(l)}(i, j)$ is obtained by finding out a point with the same intensity to $\boldsymbol{x}'^{(l)}(i, j)$ and the same saturation to $\boldsymbol{x}^{(l)}(i, j)$ as shown in Figure 3(b).

2.4. **Fusion of multi-exposure images.** The hue-corrected and saturation-preserved intensity conversion results $\boldsymbol{x}''^{(l)}(i, j)$ are merged by using saturation weighted averaging. The resultant image $\boldsymbol{y}(i, j)$ is obtained as follows:

$$\boldsymbol{y}(i, j) = \frac{\sum_{l=1}^{L} w^{(l)}(i, j) \boldsymbol{x}''^{(l)}(i, j)}{\sum_{l=1}^{L} w^{(l)}(i, j)}, \tag{9}$$

$$w^{(l)}(i, j) = \exp\left(\tau x_{\text{sat}}^{(l)}(i, j)\right). \tag{10}$$

where τ is a parameter to adjust the strength of the weighting effect by saturation.

3. **Experiment.** To verify the effectiveness of the proposed method, each method is applied to 10 sets of multi-exposure images shown in Figure 4. In this experiment, an HDR image is generated by using multi-exposure images, and these images are input to each method. As the comparison method, Inoue et al.'s method [5], Li and Kang's method [3], and Moriyama et al.'s method [6] are used. In Inoue et al.'s method [5], the parameter β is set to 0.01. In Li and Kang's method, the default parameters shown in [3] were used since these parameter settings can generate good subjective performance for most images. In Moriyama et al.'s method [6], the parameter α is set to 2. In the proposed method, the parameter τ is set to 0.01. Furthermore, the radius of the Gaussian filter r is set to be 10% of the image's short side. These parameters are experimentally decided.

In this experiment, TMQI [14] is used for quantitative evaluation. TMQI is an image quality index for evaluating LDR images using HDR images as a reference. TMQI is in the range of $[0, 1]$; the larger the value, the better the result.
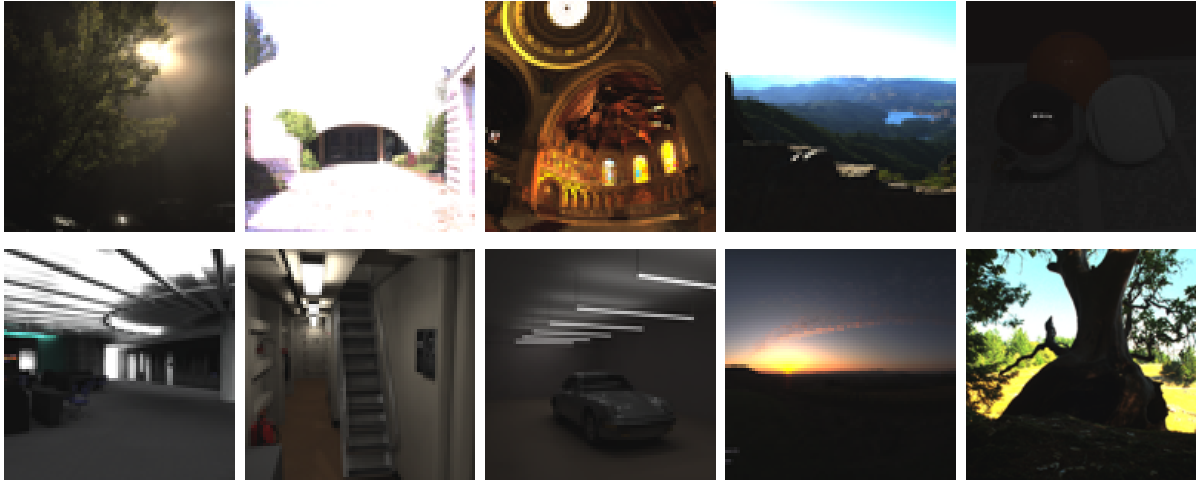
FIGURE 4. Images used in experiments

(a) Original image

(b) Inoue et al.

(c) Li and Kang

(d) Moriyama et al.

(e) Prop.

FIGURE 5. Results for "Image1": (a) original image, (b) Inoue et al. (T-MQI = 0.87), (c) Li and Kang (TMQI = 0.77), (d) Moriyama et al. (TMQI = 0.84), and (e) proposed method (TMQI = 0.88)

Figures 5 and 6 show the results of each method for "Image1" and "Image2", respectively. In the proposed method, high contrast images are obtained in comparison with conventional methods. Focusing on the enlarged image of "Image1" (Figure 5(e)), it can be seen that the contrast of the ground and trunk of the tree regions is high. In the resultant image of "Image2" (Figure 6(e)), there is no excessive enhancement or halo seen in Li and Kang's and Moriyama et al.'s methods. The regions of the grass and sky are

(a) Original image

(b) Inoue et al.

(c) Li and Kang

(d) Moriyama et al.
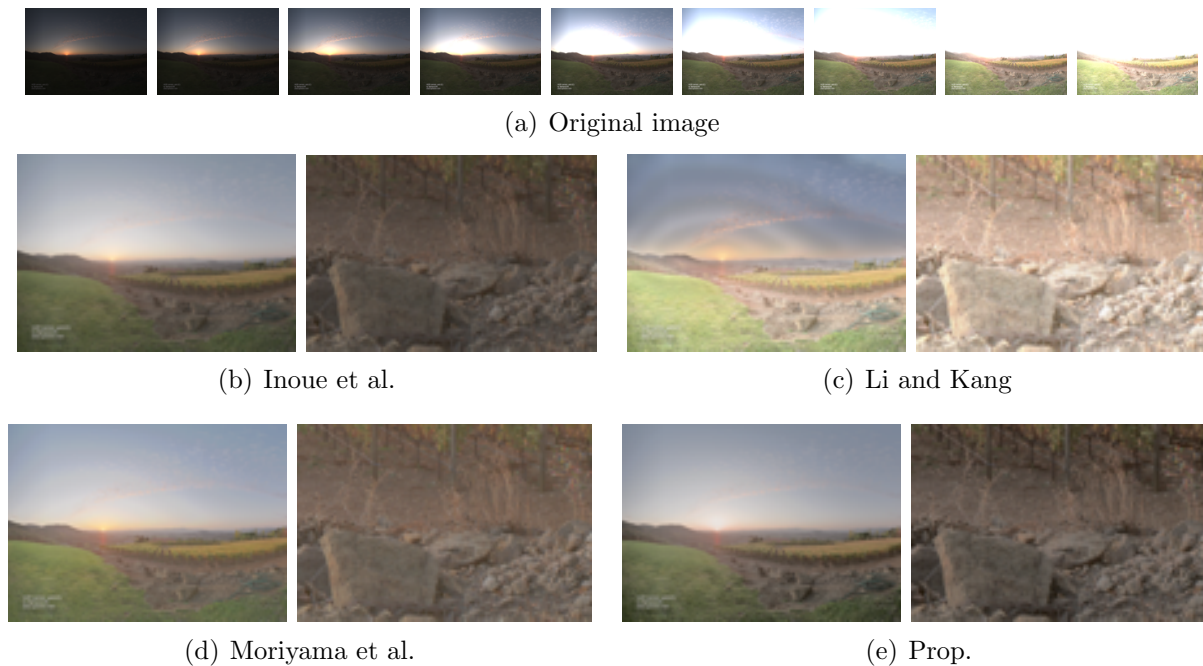
(e) Prop.

FIGURE 6. Results for "Image2": (a) original image, (b) Inoue et al. (T-MQI = 0.72), (c) Li and Kang (TMQI = 0.73), (d) Moriyama et al. (TMQI = 0.72), and (e) proposed method (TMQI = 0.73)

of good quality in the original image. The proposed method also shows the best result in the evaluation by TMQI.

4. **Conclusion.** In this letter, we proposed a novel multi-exposure image fusion method with intensity conversion using the histogram specification method. Through the experiment using some multi-exposure images, the validity and effectiveness of the proposed method were verified. The advantage is that the proposed method can prevent the occurrence of unnatural colors and obtain a well-enhanced HDR image.

Future works are to improve the weight calculation method and to develop an automatic determination algorithm of parameters.

REFERENCES

[1] S. Battiato, G. Messina and A. Castorina, Exposure correction for imaging devices: An overview, in *Single-Sensor Imaging: Methods and Applications for Digital Cameras*, R. Lukac (ed.), FL, USA, CRC Press, 2008.

[2] T. Mertens, J. Kautz and F. V. Reeth, Exposure fusion, *Proc. of Pacific Graphics, Computer Graphics and Applications*, pp.382-390, 2007.

[3] S. Li and X. Kang, Fast multi-exposure image fusion with median filter and recursive filter, *IEEE Trans. Consumer Electron*, vol.58, no.2, pp.626-632, 2012.

[4] S. Li, X. Kang and J. Hu, Image fusion with guided filtering, *IEEE Trans. Image Processing*, vol.22, no.7, pp.2874-2875, 2013.

[5] K. Inoue, H. Yu, K. Hara and K. Urahama, Saturation-enhancing multi-exposure image fusion, *The Journal of the Institute of Image Information and Television Engineers*, vol.70, no.8, pp.J185-J187, 2016 (In Japanese).

[6] D. Moriyama, Y. Ueda, H. Misawa, N. Suetake and E. Uchino, Saturation-based multi-exposure image fusion employing local color correction, *Proc. of the 26th IEEE Int. Conf. on Image Process.*, pp.3512-3516, 2019.

[7] R. C. Gonzales and R. E. Woods, *Digital Image Processing*, 3rd Edition, Pearson Education, Inc., 2008.

[8] S. M. Pizer, E. P. Amburn, J. D. Austin, R. Cromartie, A. Geselowitz, T. Greer, B. H. Romeny, J. B. Zimmerman and K. Zuiderveld, Adaptive histogram equalization and its variations, *Computer Vision, Graphics, and Image Processing*, vol.39, no.3, pp.355-368, 1987.

[9] K. Zuiderveld, Contrast limited adaptive histogram equalization, in *Graphic Gems IV*, Cambridge, Academic Press, 1994.

[10] Y. T. Kim, Contrast enhancement using brightness preserving bi-histogram equalization, *IEEE Trans. Consumer Electronics*, vol.43, no.1, pp.1-8, 1997.

[11] J. A. Stark, Adaptive image contrast enhancement using generalizations of histogram equalization, *IEEE Trans. Image Processing*, vol.9, no.5, pp.889-896, 2000.

[12] V. Teh, K. S. Kim and E. K. Wong, Contrast enhancement of CT brain images using gamma correction adaptive extreme-level eliminating with weighting distribution, *International Journal of Innovative Computing, Information and Control*, vol.14, no.3, pp.1029-1041, 2018.

[13] S. K. Naik and C. A. Murthy, Hue-preserving color image enhancement without gamut problem, *IEEE Trans. Image Processing*, vol.12, no.12, pp.1591-1598, 2003.

[14] H. Yeganeh and Z. Wang, Objective quality assessment of tone-mapped images, *IEEE Trans. Image Processing*, vol.22, no.2, pp.657-667, 2012.